Title

Climate change will accelerate the high-end risk of compound drought and heatwave events.

Journal

Proceedings of the National Academy of Sciences of USA, 120(28)

Authors

Tripathy, Kumar

Mukherjee, Sourav

Mishra, Ashok

et al.

Publication Date

2023-07-11

DOI

10.1073/pnas.2219825120

Peer reviewed

PNAS RESEARCH ARTICLE | STATISTICS

Climate change will accelerate the high-end risk of compound drought and heatwave events

Kumar P. Tripathy[a], Sourav Mukherjee[a], Ashok K. Mishra[a,1], Michael E. Mann[b], and A. Park Williams[c,d]

Edited by Hong-Yi Li, University of Houston, Houston, TX; received November 20, 2022; accepted May 6, 2023 by Editorial Board Member Jean Jouzel

Compound drought and heatwave (CDHW) events have garnered increased attention due to their significant impacts on agriculture, energy, water resources, and ecosystems. We quantify the projected future shifts in CDHW characteristics (such as frequency, duration, and severity) due to continued anthropogenic warming relative to the baseline recent observed period (1982 to 2019). We combine weekly drought and heatwave information for 26 climate divisions across the globe, employing historical and projected model output from eight Coupled Model Intercomparison Project 6 GCMs and three Shared Socioeconomic Pathways. Statistically significant trends are revealed in the CDHW characteristics for both recent observed and model simulated future period (2020 to 2099). East Africa, North Australia, East North America, Central Asia, Central Europe, and Southeastern South America show the greatest increase in frequency through the late 21st century. The Southern Hemisphere displays a greater projected increase in CDHW occurrence, while the Northern Hemisphere displays a greater increase in CDHW severity. Regional warmings play a significant role in CDHW changes in most regions. These findings have implications for minimizing the impacts of extreme events and developing adaptation and mitigation policies to cope with increased risk on water, energy, and food sectors in critical geographical regions.

drought | heatwaves | compound drought and heatwaves | CMIP6

Significance

Compound drought and heatwaves (CDHWs) severely threaten socioecological systems, leading to greater impacts, e.g., wildfires, crop failure, and heat-related mortalities, than individual extremes. This topic is timely as we witnessed severe CDHW events in California and the southwest United States, Europe, and China in 2022, while the "black summer" of 2019/2020 in Australia remains a profound example of this threat. This study investigated the high-end risk of CDHW under climate change and the potential role of global and regional warming thresholds on the high-end risk of CDHW events. Roughly 20% of global land areas will likely observe ~2 CDHW events/year that last ~25 d by the late 21st century based on the high-end scenario.

Compound drought and heatwaves (CDHWs) pose a severe threat to socioecological systems (1, 2), leading to greater impacts, e.g., wildfires (3), agriculture (4–6), massive heat-related mortalities (7, 8), and socioeconomic catastrophes (9), than individual extremes (10). In recent decades, CDHWs have increased globally (11), including Europe (12–14), the United States (15), South America (16), Australia (17, 18), and Asia (19–22).

Droughts and heatwaves are often governed by interconnected processes that produce coupled changes in precipitation and temperature (23–25) due to enhanced sensible heat flux at the expense of latent heat flux arising from positive land-atmosphere feedbacks that involve changing land and vegetation cover (26, 27). Although natural variability is responsible for the CDHWs (26), previous studies have highlighted that the human-caused warming has intensified the drivers, resulting in more persistent droughts and heatwaves across widespread regions (11, 28). Previous work investigated CDHWs (11) based on recent observed periods and record-shattering heatwaves (29) under future climate change scenarios; however, a holistic analysis exploring high-end risk related to such compound events for projected climate scenarios remains underexplored.

This article first explores the projected spatiotemporal shifts in CDHW characteristics (frequency, duration, and severity) across different climate regions under future warming scenarios using recent observations as the baseline. Second, we investigate the spatial evolution of high-end risk of CDHW under climate change, and third, the role of global and regional warming thresholds on high-end risk of CDHW events is investigated for twenty-six climate divisions.

We make use of daily maximum 2 m air temperature (Tmax) and weekly self-calibrated palmer drought severity index (sc-PDSI) to evaluate joint heat/drought CDHW metrics based on bias-corrected simulation outputs from eight models from the Coupled Model Intercomparison Project 6 (CMIP6) to quantify the projected changes in CDHW event characteristics for three future emission scenarios relative to the baseline recent observed period (1982 to 2019). We examine the changes in CDHW characteristics (frequency, duration, and severity) over altered evaporation regimes for selected thresholds of global temperature increase at 0.5 °C intervals from 0.5 °C to 3.5 °C. The results identify a number of global hotspots of projected increase in high-end CDHW risk. Our findings offer implications for societal exposure to an array of climate impacts on water resources, ecosystem health, economic stability, and societal welfare.

Author affiliations: [a]School of Civil and Environmental Engineering and Earth Sciences, Clemson University, Clemson, SC 29634; [b]Department of Earth & Environmental Science University of Pennsylvania, Philadelphia, PA 19104-6316; [c]Department of Geography, University of California, Los Angeles, CA 90095; and [d]Lamont-Doherty Earth Observatory of Columbia University, Palisades, NY 10096

Author contributions: A.K.M., K.P.T., and S.M. designed research; K.P.T. and S.M. performed research; K.P.T. and S.M. analyzed data; A.P.W. review and editing; and K.P.T., S.M., A.K.M., M.E.M., and A.P.W. wrote the paper.

The authors declare no competing interest.

This article is a PNAS Direct Submission. H.-Y.L. is a guest editor invited by the Editorial Board.

[1]To whom correspondence may be addressed. Email: ashokm@g.clemson.edu.

This article contains supporting information online at https://www.pnas.org/lookup/suppl/doi:10.1073/pnas.2219825120/-/DCSupplemental.

Published July 3, 2023.

Results

Historical and Projected Global Changes in CDHW Characteristics. We investigated trends during both the recent observed and future periods in global CDHW characteristics (frequency, duration, and severity) and spatial extent therein based on the multimodel ensemble (MME) mean of eight climate models from the CMIP6 (Fig. 1). CDHW frequency, duration, and mean annual severity (hereafter, severity) are calculated using a methodology (*Materials and Methods*) previously applied in Mukherjee and Mishra (11).

Fig. 1 *A*–*C* depicts the yearly time series of CDHW frequency, duration, and severity for the recent observed (1982 to 2019), near-future (2020 to 2057), and far-future (2058 to 2095) periods. The near-future and far-future projections correspond to three shared socioeconomic pathway (SSP) scenarios: low-end emissions (SSP1-2.6), mid-range emissions (SSP2-4.5), and high-end emissions (SSP5-8.5) scenarios. An area correction method is applied to each grid point (refer to *SI Appendix*, section A3) to account for the latitudinal changes in the grid area. The 5 to 95% range characterizes the intermodel spread among all GCM projections, as depicted by the shading in Fig. 1 *A*–*C*. The yearly values are derived by taking the spatially weighted average of the annual time series obtained for individual grids across the global land surface. We identify statistically significant trends in the CDHW characteristics time series based on the nonparametric Mann–Kendall's test (refer to *SI Appendix*, section A4). Results demonstrate significant trends in all the scenario-period combinations, with exceptions being in the low-end emissions scenario (SSP1-2.6; *SI Appendix*, Table S2), indicating stronger CDHW activity in the future.

Models project a global average increase in frequency, duration, and severity of CDHW events throughout the 21st century. Under the SSP5-8.5, it is projected that the number of CDHW events is likely to increase by ~2.5 (1.5) per year, with an average duration up to ~25 (10) days and severity of each event increasing ~130 (50) by the end of far future (near-future). This translates to an approximately threefold increase in frequency, fivefold increase in duration, and fourfold increase in severity by the end of the 21st century relative to year 2019. A significant increasing pattern in CDHW characteristics is projected for the high emission scenario (SSP5-8.5) followed by moderate (SSP2-4.5) scenarios compared to the mild (SSP1-2.6) scenarios, which is consistent with recent literature (21, 30).

Fig. 1 *D*–*F* illustrates the smoothed (7-y moving mean) variation of the CDHW event characteristics exceeding different areal thresholds (20%, 40%, 60%, and 80% of global land areas) for the recent observed and SSP5-8.5 scenario. The procedure implemented for defining areal thresholds and Fig. 1 *D*–*F* are provided in supplementary section A5. On average, the top 20% of most affected land areas are projected to experience ~3 CDHW events/year that can last for ~30 d/year with a severity of ~130 by the end of the 21st century under the SSP5-8.5 scenario. This is a considerable increase from the recent observed period (1982 to 2019), for which the 20% of most affected land area experienced only ~1 event/year with less than 10 d of duration and severity of ~40.

Projected Changes of CDHW at Regional Scales. We explore the projected changes in frequency, duration, and severity across 26 global climate divisions (proposed by IPCC-AR5; refer to

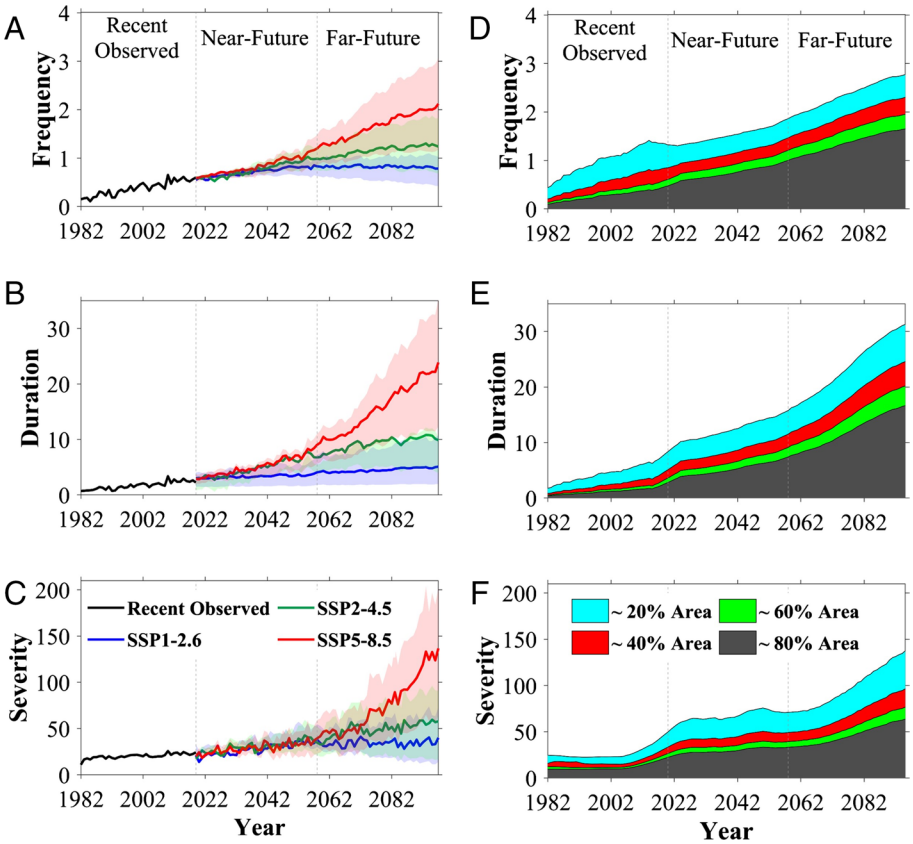

Fig. 1. Historical and projected global changes in CDHW characteristics: (*A*–*C*) Variation in observed and GCM-based MME mean projections of summer CDHW characteristics—(*A*) frequency, (*B*) duration, and (*C*) severity—spatially averaged over the globe for recent observed period (1982 to 2019) and model simulated future period (2020 to 2099) based on the selected future climate scenarios (SSP1-2.6, SSP2-4.5, and SSP5-8.5). The shading represents the intermodel variability or spreads based on 5 to 95th percentile bounds, and (*D*–*F*) 7-y moving average of CDHW characteristics—(*D*) frequency, (*E*) duration, and (*F*) severity—for four different areal thresholds (20%, 40%, 60%, and 80%) based on recent observed and SSP5-8.5 scenario.

SI Appendix, Fig. S1) based on the MME mean projections from eight CMIP6 GCMs. The changes in CDHW characteristics are evaluated for the near-future (2020 to 2057) and far-future (2058 to 2095) periods relative to the recent observed period (1982 to 2019) for individual grid locations. We evaluated the average increase in CDHW frequency (by taking spatial weighted average of change in frequency) in the SSP5-8.5 scenario for the far future relative to the baseline recent observed period across 26 climate divisions as represented by bar plots in Fig. 2*A*. For continental-based assessments of the changes in CDHW characteristics, these bar plots are grouped by continent. The results suggest that East Africa, Central Asia, North Australia, Central Europe, Southeastern South America, and East North America are the six climate regions with the largest future increase (hotspots) in the CDHW frequency within each continent due to the contribution of anthropogenic warming as per the SSP5-8.5 scenario in the far future. We summarized the spatial distribution of changes in CDHW characteristics for these six climate regions using boxplots in Fig. 2 *B*–*G*. The results for the rest of the 20 climate regions are provided in *SI Appendix*, Fig. S5. The absolute values of the CDHW characteristics are illustrated by the spatial maps shown in *SI Appendix*, Figs. S2–S4.

Model simulations show that with increased future emissions, these climate hotspots are most likely to experience increased occurrences of CDHW events by the end of the century, especially in the SSP5-8.5. Among the six regions already found to have the largest projected increases in CDHW frequency on each continent, East Africa and North Australia are the two regions with the largest increases on the globe. For example, an increase of ~2 to 3 events, ~25 to 35 d with ~30 to 50 severity observed in the Southeast South America; and an increase of ~2 to 3.5 events, ~12 to 20 d, and ~ 40 to 50 severity in Central Asia under the SSP5-8.5 scenario in the far future. Similarly, Central Europe is likely to experience an increase of ~0.5 to 2 events, ~5 to 20 d, and ~20 to 40 in the severity of CDHW events. A key difference in CDHW characteristics in North America is noteworthy between East North America and West North America. Although East North America is projected to experience more CDHW events, the median severity of the CDHW events in West North America under the SSP5-8.5 scenario in the far future is significantly higher than that of the East North America (*SI Appendix*, Fig. S5 and Fig. 2). The difference in CDHW trends in the eastern and western parts of North America likely comes about because of contrasting mean climatologies and precipitation projections, as annual precipitation totals are projected to increase in the already relatively wet East North America more than across much of the already arid West North America (31) (*SI Appendix*, Fig. S6). Warming in West North America thus causes CDHWs to be on average more severe and longer lasting while precipitation increases in the east often offset the CDHW-promoting effects of warming (32).

Furthermore, we analyzed the spatial asymmetry of the CDHW characteristics by exploring their latitudinal variations (*SI Appendix*, Fig. S7). The results suggest that the midlatitudes are where

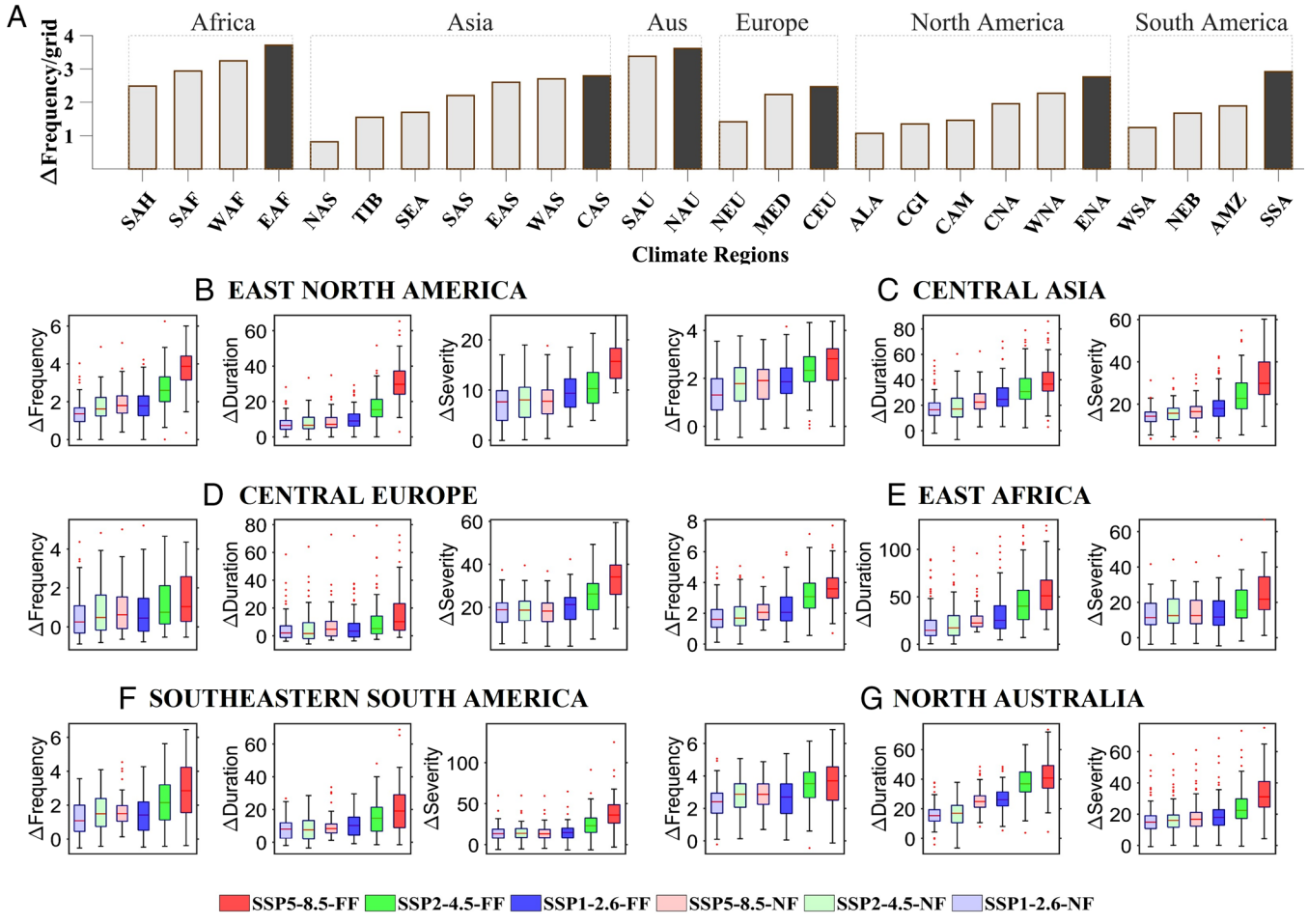

Fig. 2. Projected changes of CDHW at regional scales: (*A*) The bar plot indicates the average increase in CDHW frequency relative to the recent observed period (1982 to 2019) across 26 climate divisions. The black bars indicate the climate division with the highest average increases within each of the six continents. (*B*–*G*) Boxplots show the spatial distribution of change in the three CDHW characteristics in the future climate scenarios relative to the recent observed period (1982 to 2019) across the six hotspot climate divisions identified in *A*.

models project CDHW activity to increase the most in terms of frequency, duration, and severity. Comparing hemispheres, models project the Southern Hemisphere to experience larger increases in CDHW event frequency while they project CDHW severity to increase more in the Northern Hemisphere. Overall, such latitudinal variation in CDHW characteristics may be driven by intensified land-atmosphere feedbacks (27, 33) and changes in El Niño-Southern Oscillation (ENSO) patterns (34–37) and, therefore, warrants further investigation.

Mapping the High-End Risk of CDHW Events in Future Climate Scenarios. Quantifying the spatial risk of climate extremes under climate change is valuable for developing adaptation strategies. Here, we perform a frequency-based analysis to investigate the spatial evolution of the risk of CDHW events in future climate scenarios. The frequency of high-end risk of CDHW events is determined based on specific return intervals (or periods) considering the future events that are more severe and longer duration compared to the recent observed period (*Materials and Methods*). Finally, the spatial evolution of high-end risk of CDHW events is investigated based on area–frequency curves (*SI Appendix*, section A6). This analysis allows us to investigate how the frequency–area relationship of CDHW events, potentially more severe and longer than the recent observed period, will change due to anthropogenic warming.

Area–frequency curves (Fig. 3) are derived for each of the six hotspot climate divisions for the far-future (2058 to 2095) period based on the three future climate scenarios. The area–frequency curves for the remaining 20 climate divisions are shown in *SI Appendix*, Fig. S8. The results suggest an increase in the areal extent of high-end risk of CDHW events due to a rise in anthropogenic warming across all six hotspot climate divisions. This indicates a more significant percentage of areal extent notable in the SSP5-8.5 scenario in the far future for any given return period (RP). For instance, in the North Australia region, 1-y CDHW events are likely to affect more than 60% area in the highest (SSP5-8.5) emission scenario compared to 40% in the moderate (SSP2-4.5) emission scenario during the far-future period. Similarly, for Southeast South America, 5-y CDHW events are likely to affect 30% area under the SSP5-8.5 scenario in the far-future period as compared to 20% and 25% area in the low and moderate emission scenarios. Across East North America, 2-y CDHW events are likely to affect more than twofold based on the SSP5-8.5 and SSP2-4.5 scenarios and ~1.5-fold (SSP1-2.6) compared to the recent observed period. These results highlight the necessity of planning and mitigation efforts that may have implications for the ecosystem adaptability due to the emergence of CDHW events whose duration and severity have no analog in the present climate.

Impact of Global and Regional Warming Thresholds on High-End Risk of CDHW Events. As the globe warms, most land areas are projected to warm more rapidly, with much regional variation in warming rates. Geographic variations in warming rates should contribute to geographic variations in how CDHW risks evolve in the future. We illustrate this disproportionate historical and future warming for the six hotspots where CDHW frequency is projected to increase most rapidly in the Fig. 4 bar plots (also shown in *SI Appendix*, Fig. S9 for rest of the twenty climate divisions). These bar plots demonstrate the association of change in global mean temperature anomalies with the difference between global and regional temperatures for the hotspot climate divisions. Different regions show a variety of disproportionality based on the temporal trends in the difference in anomalies that varies for different climate divisions. These disproportionate regional temperature increases can be attributed to possible intensification of land-atmosphere feedbacks and shifts in teleconnection patterns

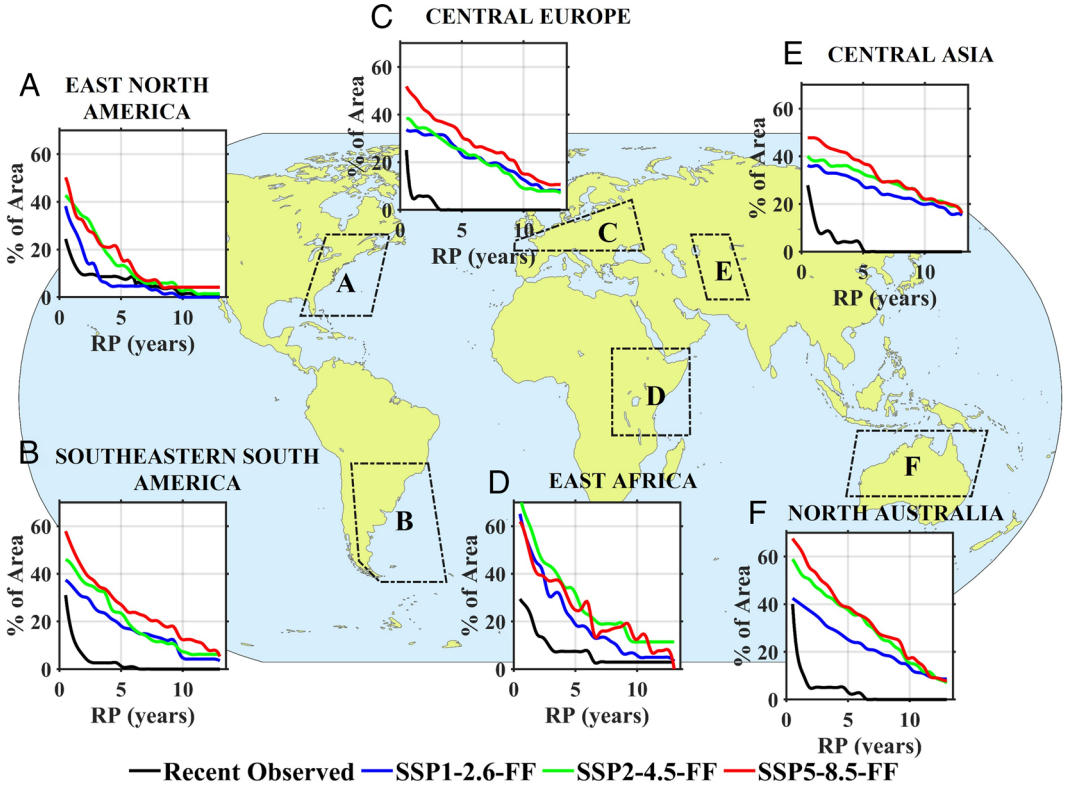

Fig. 3. Spatial Evolution of High-End Risk of CDHW under Climate Change: (*A–F*) Area–frequency curves for (*A*) East North America, (*B*) Southeastern South America, (*C*) Central Europe, (*D*) East Africa, (*E*) Central Asia, and (*F*) North Australia are shown recent observed period (1982 to 2019) and for the model simulated far future (2058 to 2095) based on the three future climate scenarios. The curves are smoothened using a 7-y moving mean.

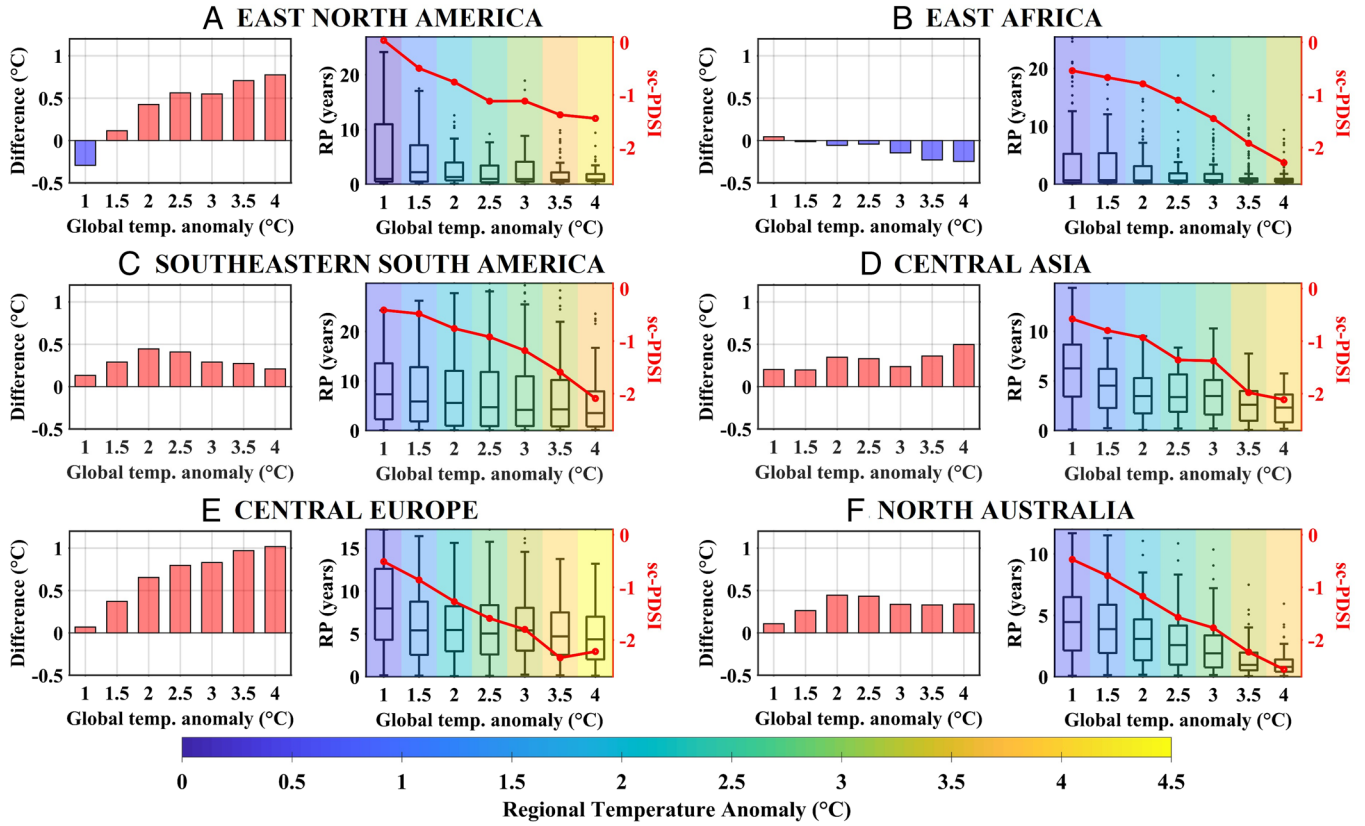

Fig. 4. Impact of global and regional warming thresholds on high-end risk of CDHW events: (*A*–*F*) Bar plots show the difference between global and regional mean temperature anomalies at different global warming levels across (*A*) East North America, (*B*) East Africa, (*C*) Southeastern South America, (*D*) Central Asia, (*E*) Central Europe, and (*F*) North Australia. The boxplots indicate the return periods of CDHW events as a function of global (*x* axis) and regional temperature anomalies (shading) and sc-PDSI (drought magnitude; right *y* axis). The return periods are estimated for a 31-y window centered on the year when the global mean temperature anomaly permanently exceeds a particular warming threshold.

in response to mean global warming (38, 39). However, all climate divisions, except East Africa, show that regional warming is likely to exceed global warming for any threshold of global temperature anomalies in the SSP5-8.5 scenario, consistent with IPCC AR6 (2021; https://www.ipcc.ch/report/ar6/wg1/resources/factsheets/).

We investigate the association between the high-end risk of CDHW events in response to the disproportionate rise in global and regional warming levels (or thresholds) in the SSP5-8.5 scenario. RPs of CDHW events, representing the high-end risk, are estimated using the MME mean of historical model runs and future projections for 31 y corresponding to a given warming threshold (*Materials and Methods*). For example, a 1.5 °C warming threshold refers to a 31-y period, which includes 15 y before and 15 y after the specific year when the MME mean of the global mean temperature anomaly permanently crosses the +1.5 °C threshold. Once this 31-y window is selected for a given warming threshold, the RPs for high-end risk events are calculated for that period based on the MME mean of CDHW characteristics (*Materials and Methods*) for the gridded locations. The spatial distribution of the RPs for subsequent increases in global temperature anomalies is depicted by boxplots in Fig. 4. We further link these RPs and global mean temperature anomalies with the corresponding regional temperature anomalies and drought severity (sc-PDSI magnitudes shown by a solid red line) as demonstrated in Fig. 4.

A significant decrease in RPs with an increase in the global and regional warming levels can be noted in the SSP5-8.5 climate scenario across all six climate divisions. This indicates that the severity and duration of historically most extreme CDHW events in the recent observed period are likely to become more frequent in the future climate due to anthropogenic warming. However, Fig. 4 indicates considerable heterogeneity across climate divisions in response to disproportionality between global and regional warming in the future climate. For example, the median RP can decrease from ~4.5 to ~1 y and ~8 to ~5 y with increased global warming from 1 °C to 4 °C in North Australia and Central Europe, respectively. The upper quartile of RP can drop significantly from ~4 to ~1 y across East Africa. The area-averaged mean sc-PDSI values (right *y* axis) illustrate that as the mean sc-PDSI decreases, a more significant proportion of the region will likely experience drought conditions with increased global warming. Furthermore, the projected mean sc-PDSI values (solid red line) decline monotonically with increased global mean temperature anomalies for most climate divisions.

Overall, the results from the analysis demonstrate the rise in the risk of CDHW events in the future due to continued anthropogenic warming. Most climate divisions show a possible rise in risk of CDHW events accompanied by higher regional warming relative to global warming, indicating a potential role of increased land-atmosphere feedbacks in the region, which needs further attention. On the contrary, less regional warming across East Africa, Central Asia, West Africa, and South Australia indicates that large-scale teleconnections such as stronger La Niña or El Niño states (34–37) and temperature responses to increasing precipitation may play a role in modulating the increase in hot extreme events in some regions.

Although our study primarily focuses on the high-end risk of CDHW events and their associations with global and regional warming levels, we recognize the importance of understanding the underlying mechanisms, such as land-atmosphere feedbacks, shifts in teleconnection patterns, and large-scale teleconnections

like La Niña or El Niño states (40), that could contribute to these changes. While there is existing literature that supports the role of these mechanisms in modulating extreme events, a detailed investigation and direct evidence of these mechanisms goes beyond the scope of this paper. We encourage future research to explore these mechanisms in greater detail to improve our understanding of the factors driving the projected changes in CDHW events.

Discussion

Our analysis found increases in compound drought and heatwave (CDHW) characteristics (frequency, duration, and severity) in the near- and far future under various scenarios of future warming. The increases are most pronounced in key vulnerable geographical regions, underscoring the potential impacts on large, vulnerable populations, socioeconomic systems, and ecosystems. The intensified CDHW characteristics are largest in the high-end SSP5-8.5 and moderate in the SSP2-4.5 scenario. The results suggest that taking the SSP2-4.5 path would lead to large and important mitigation of CDHW trends compared to the SSP5-8.5 path. In the high-end scenario, roughly 20% of global land areas are likely to observe ~2 CDHW events/year that last ~25 d with a severity of ~130 by the late 21st century. For comparison, the average over the recent observed reference period is ~1.2 events/year, <10 d/year, with a severity of ~40, respectively. The substantial increase in CDHW characteristics highlights the profound threat of more frequent and intense CDHW events in the upcoming decades, depending on the emissions pathway followed.

Past studies indicate that global climate change causes disproportionate surface energy partitioning over many regions and amplifies compound extremes (27, 41). Soil moisture memory adds to the persistence of compound drought/heatwave events (42). Because current generation climate models fail to accurately reproduce the planetary wave resonance conditions that have been implicated in the increase in persistent summer weather extremes (43–45), our analysis may underestimate the potential for increased duration CDHW events.

Analyzing spatiotemporal shifts in projected CDHW characteristics across 26 climate divisions, we found that East North America, Southeast South America, Central Europe, East Africa, Central Asia, and North Australia (six "hotspot" regions) are likely to witness the largest increase in the frequency of CDHW events as per the SSP5-8.5 scenario in the far future. Recent studies have suggested that these hotspot regions may be particularly vulnerable to the impacts of climate change due to a combination of factors, including their geographic location, susceptibility to changes in precipitation patterns, local hydrological processes, and reduction in soil moisture content. In East Africa, the increase in the sea surface temperature anomalies in the southwest Indian Ocean is likely to be associated with reduced moisture transport and increasing long-term dryness over many parts of East Africa (46–48). Central Asia is characterized by high aridity, making it particularly sensitive to changes in precipitation and temperature, which could contribute to increased CDHW risks. In Australia, the concurrence of strong El Nino and positive Indian Ocean Dipole (IOD) phases can bring frequent and severe CDHW conditions (49).

In the Southeastern part of South America, changes in the position and strength of the south Atlantic high-pressure system and increased El Niño-Southern Oscillation events are likely to play a key role in driving changes in precipitation patterns and drought occurrence over South America (40, 50). In East North America and Central Europe, changes in the jet stream and persistent blocking patterns can amplify regional heatwaves, while land-atmosphere feedbacks, soil moisture deficits, and changes in evapotranspiration can exacerbate the impacts of heatwaves and droughts. Further research is needed to understand these driving mechanisms and their influence on the spatial distribution of CDHW events under future warming scenarios.

The latitudinal variations of CDHW characteristics suggest that the Southern Hemisphere is likely to experience a larger increase in the frequency of CDHW events, whereas the Northern Hemisphere is likely to experience a larger increase in the severity of CDHW events, especially within the midlatitude region. Given the substantial current uncertainties in model-based projections of future ENSO behavior, including even the sign of the response of ENSO to anthropogenic forcing (51), there are important caveats in interpreting the projected changes in these regions. Quantification of high-end risk of CDHW events under climate change is often challenging. Our study has a few limitations, including the coarse resolution used in the analysis and the limited number of high-end CDHW events for RP analysis. Weekly analysis of CDHW events can partly overcome the limitations of data lengths. Future studies can investigate the role of the high-end risk of CDHW events on multiple sectors that affects socioeconomic systems. Multiple reanalysis datasets (52) can be used to quantify the uncertainties associated with high-end CDHW events. Although our study reveals that high-end CDHW events are likely to increase under climate change, more studies are needed to investigate potential mechanisms that trigger such compound extremes. The potential mechanisms are associated with land-atmosphere feedbacks, shifts in teleconnection patterns, increase in anthropogenic activities (e.g., urbanization), and the changes in quantity and seasonality (variability) of the global hydrologic cycle (53). Furthermore, continued advancements in understanding ENSO responses to anthropogenic forcing and developing more accurate climate model simulations will help improve projections of CDHW events in regions affected by ENSO variability.

The area–frequency analysis shows that the areal extent of CDHW events increases with emission rates. While certain regions such as East Africa, West Africa, and South Australia show relatively low projected warming, they still experience hot extremes in association with El Niño and La Niña events, underscoring the importance of reducing current uncertainties in projected changes in ENSO behavior and its teleconnections. We analyzed the role of regional warming trends in affecting the frequency of CDHW events. Our results strongly suggest that regional warming levels play a significant role in their occurrences, except in East Africa. Alizadeh et al. (54) also explained that the excessive heat caused due to intense-land-atmospheric feedback is the dominant driver of the compound dry and hot events.

Because of the disparate impacts of CDHW frequency and severity across societal and ecological sectors, our findings offer important implications for stakeholders and policymakers in the areas of hydrology and water resources, forest management, the energy sector (55), socioeconomic disciplines (56, 57), agricultural sectors (4), health sciences (58), and ecology and wildlife protection (59), providing guidance for planning, preparing, and mitigating adverse climate change impacts in these sectors. Future research focusing on quantifying the influence of land use and land cover on moisture transport and heat advection, and land-atmosphere feedbacks, and in constraining large-scale teleconnection patterns should help further elucidate the factors underlying increased CDHW-related climate change risk.

Materials and Methods

Data. Daily observed precipitation is obtained from the Global Precipitation Climatology Centre (GPCC) for the period 1982 to 2019, available at $1^o \times 1^o$ spatial resolution. Daily observed maximum and minimum 2 m air temperature

datasets (T_{max} and T_{min}) for the same period are downloaded from the Climate Prediction Center (CPC), which are available at 0.25° spatial resolution for the globe. In addition, we also analyzed CDHW characteristics for the future periods using eight general circulation model (GCM; *SI Appendix*, Table S1) outputs of precipitation flux, T_{max}, and T_{min} under three SSP-representative concentration pathway (SSP-RCP: SSP1-2.6, SSP2-4.5, and SSP5-8.5) scenarios from the latest CMIP6 (available at https://esgf-node.llnl.gov/projects/cmip6/). The GCM outputs obtained for the future period are bias corrected by employing a nonstationary bias-correction technique (60) with respect to the corresponding historical model runs and observed datasets (explained in *SI Appendix, Appendix A1*). We performed a correlation analysis using precipitation, temperature data, and CDHW characteristics between GPCC and bias-corrected GCM model outputs to identify the best GCMs. Based on this analysis, we selected 8 GCMs to investigate further climate change's potential influence on CDHW characteristics at a global scale. The GCM outputs were selected considering a single realization (*r1i1p1f1*).

All datasets (both observations and GCM outputs) are first regridded to $2^o \times 2^o$ spatial resolution by applying bilinear interpolation. An Available Water Content (AWC) dataset, which is a parameter for the sc-PDSI, was retrieved from a soil texture-based global water-holding-capacity map produced by Webb et al. (61) and extracted at 2^o spatial resolution. In this study, only land areas between 66^oN and 66^oS are considered.

Estimation of CDHW Characteristics. First, drought events are derived based on the weekly sc-PDSI, which is calculated by following the procedure proposed in Wells et al. (62). A drought week is defined when the weekly sc-PDSI magnitude falls below the 10th percentile calculated for the entire study period. In this study, a heatwave event is decided when the daily Tmax exceeds the 95th percentile of the summer daily Tmax for at least three consecutive days. Two heatwave events are considered independent if they are separated by more than 4 d; otherwise, they are considered a single event.

This study focuses on three main CDHW characteristics: frequency, duration, and severity for the summer months (May–October in the Northern hemisphere and November–April in the Southern Hemisphere). The CDHW characteristics are calculated by combining the drought (weekly sc-PDSI) and heatwave (daily maximum temperature) metrics (refer to *SI Appendix*, Fig. S10). A compound drought and heatwave event occur $(CDHW_i)$ when both heatwave (H_i) and a drought (D_i) episodes occur simultaneously, i.e., $(H_i = 1 \cap \ D_i = 1)$ for a grid i. Mathematically,

$$CDHW_i = \begin{cases} 1, & (H_i = 1 \cap D_i = 1) \\ 0, & otherwise \end{cases}. \qquad [1]$$

The three CDHW characteristics are calculated as follows: a) frequency, defined as the average number of CDHW events for a given year; b) duration, defined as the total number of CDHW event days occurred for a given year; and c) CDHW severity for an individual event is calculated based on the cumulative sum of the daily severity values obtained over the consecutive days of the CDHW event. Daily severities are estimated as the product of the daily standardized values of maximum temperatures and the sc-PDSI value of the coinciding extreme drought week. Then, the mean annual CDHW severity ("severity" in the main text) is calculated as the average of all the year's event severities. See *SI Appendix, Appendix A2* for calculation of severity.

We constructed the MMEs of three CDHW characteristics by considering the arithmetic mean of the eight GCMs separately for the three scenarios (SSP1-2.6, SSP2-4.5, and SSP5-8.5) as the MMEs of the GCMs perform better by capturing the temporal changes efficiently compared to the individual models (63).

Calculation of RPs. We represent the high-end risk of CDHW events in the future periods based on RPs calculated for the six future climate scenario–period combinations. Specifically, the RPs are calculated as the reciprocal of the joint probabilities of occurrences of CDHW events with slight modification to the methodology suggested by Ridder et al. (64). To focus on the high-end risk of CDHW events in our analysis, the estimation of RPs is based on events that are likely to be equally or more severe and more extended in the future than observed in the recent observed period. As such, a conditional approach is adopted based on the following two criteria.

1. The events should have lasted for at least the maximum number of CDHW days in the observation.
2. For that event, the severity values should exceed the maximum daily severity evidenced in the observation.

This approach explicitly focuses on the high-end risk with prolonged and severe CDHW events in the future, which was never addressed in the previous joint compound extreme studies. First, the joint occurrence probability of the CDHW events (satisfying the above two criteria) for every grid cell (*lat, lon*) and future climate scenario (*SSP*) was calculated as the MME mean of the total CDHW days divided by the total number of summer days for that period, given as,

$$P(H \cap D | d_f \geq d_p, S_f \geq S_p)_{SSP,lat,lon} = \frac{\left(\sum_{n=1}^{N} \sum_t CDHWd\left(t, lat, lon, SSP | d_f \geq d_p, S_f \geq S_p\right)/N\right)}{\sum_t Summerdays(t, lat, lon)}, \qquad [2]$$

where $P(H \cap D | d_f \geq d_p, S_f \geq S_p)_{SSP,lat,lon}$ denotes the conditional joint probability; d_p and S_p are the maximum duration and severity of CDHW event in the present period for grid location (*lat, lon*); d_f and S_f are the duration and severity of CDHW event for the grid location (*lat, lon*) in the future climate scenario, *SSP*; and N is the total number of CMIP6-GCMs used in the study.

Finally, the RP is calculated by standardizing the inverse of the conditional probability by number of days per year as (64).

$$RP_{SSP,lat,lon} = \frac{1}{P(H \cap D | d_f \geq d_p, S_f \geq S_p)_{SSP,lat,lon} \times 365}. \qquad [3]$$

Estimation of Global and Regional Warming Levels. First, we evaluate the global mean temperature for the recent observed period and then temporally average it to get a single value. This value represents the global mean temperature over the recent observed or climatological period (1982 to 2019).

$$T_{climatological\ mean} = \sum_{t=1982}^{2019} \sum_{\forall\ grids} T_{mean},$$

where T_{mean} represents the mean temperature series over the globe, i.e., average of T_{max} and T_{min}.

Then, we calculated the global mean–annual temperature anomalies as follows:

1. Concatenate the global mean surface air temperature (T_{mean}) for recent observed period and the SSP5-8.5 for all the GCM models to get the full time series of global temperature from 1982 to 2099.
2. Subtract $T_{climatological\ mean}$ from the concatenated series for all the models to get the anomaly series for each of the models.
3. Construct the multimodel mean ensemble (MME) by giving equal weights to the different climate models to get the global mean temperature anomaly series.

The preindustrial period (1850 to 1900) is commonly used as a benchmark to represent preindustrial temperature, which is widely used in climate change analysis. Studies have shown that the recent observed period is ~0.6 °C warmer than the preindustrial period (65). Therefore, we added an adjustment factor 0.6 °C to the multimodel mean ensemble (MME) global mean temperature anomalies to assess their relative warming levels to the preindustrial era (66).

Then, we extracted the years ("central years") for different global warming levels (1 °C, 1.5 °C, 2 °C, 2.5 °C, 3.5 °C, and 4 °C), when global mean temperature anomaly exceeds the desired warming level (67). After that, we considered the period for each of the warming levels as a 31-y window (15 y before and 15 y after the central year). We calculated the area-averaged summer mean sc-PDSI values and the RPs for each of the grid points for these 31-y periods for all 26 climate regions. The area-averaged regional temperature anomalies for all the climate regions are evaluated.

Data, Materials, and Software Availability. The datasets used in this study are publicly available from different sources. The daily observed precipitation dataset

is obtained from the Global Precipitation Climatology Centre (GPCC), accessible at https://opendata.dwd.de/climate_environment/GPCC/full_data_daily_v2020/. Daily observed maximum and minimum 2m air temperature datasets are obtained from the Climate Prediction Centre (CPC) database, which is accessible at https://psl.noaa.gov/data/gridded/data.cpc.globaltemp.html. General Circulation Model (GCM) outputs from the CMIP6 experiments can be downloaded from the https://esgf-node.llnl.gov/projects/cmip6/.

ACKNOWLEDGMENTS. This study was supported by the NSF award # 1653841 and by NOAA MAPP NA19OAR4310278.

1. N. K. Ruehr, R. Grote, S. Mayr, A. Arneth, Beyond the extreme: Recovery of carbon and water relations in woody plants following heat and drought stress. *Tree Physiol.* **39**, 1285–1299 (2019).
2. I. Ibáñez *et al.*, Forest resilience under global environmental change: Do we have the information we need? A systematic review. *PLOS One* **14**, e0222207 (2019).
3. J. Ruffault, T. Curt, N. K. Martin-StPaul, V. Moron, R. M. Trigo, Extreme wildfire events are linked to global-change-type droughts in the northern Mediterranean. *Nat. Hazards Earth Syst. Sci.* **18**, 847–856 (2018).
4. M. Zampieri, A. Ceglar, F. Dentener, A. Toreti, Wheat yield loss attributable to heat waves, drought and water excess at the global, national and subnational scales. *Environ. Res. Lett.* **12**, 064008 (2017).
5. Y. Lu, H. Hu, C. Li, F. Tian, Increasing compound events of extreme hot and dry days during growing seasons of wheat and maize in China. *Sci. Rep.* **8**, 16700 (2018).
6. H. A. Hussain *et al.*, Interactive effects of drought and heat stresses on morpho-physiological attributes, yield, nutrient uptake and oxidative status in maize hybrids. *Sci. Rep.* **9**, 3890 (2019).
7. D. Mitchell *et al.*, Attributing human mortality during extreme heat waves to anthropogenic climate change. *Environ. Res. Lett.* **11**, 074006 (2016).
8. X. Wu, D. Jiang, Probabilistic impacts of compound dry and hot events on global gross primary production. *Environ. Res. Lett.* **17**, 034049 (2022).
9. W. Steffen, K. Mallon, T. Kompas, A. Dean, M. Rice, Compound costs: How climate change is damaging Australia's economy. https://apo.org.au/node/234731 (2019).
10. J. Zscheischler *et al.*, Future climate risk from compound events. *Nat. Clim. Change* **8**, 469–477 (2018).
11. S. Mukherjee, A. K. Mishra, Increase in compound drought and heatwaves in a warming world. *Geophys. Res. Lett.* **48**, e2020GL090617 (2021).
12. M. Ionita, D. E. Caldarescu, V. Nagavciuc, Compound hot and dry events in Europe: Variability and large-scale drivers. *Front. Clim.* **3**, 688991 (2021).
13. C. Manning *et al.*, Increased probability of compound long-duration dry and hot events in Europe during summer (1950–2013). *Environ. Res. Lett.* **14**, 094006 (2019).
14. Y. Markonis *et al.*, The rise of compound warm-season droughts in Europe. *Sci. Adv.* **7**, eabb9668 (2021).
15. O. Mazdiyasni, A. AghaKouchak, Substantial increase in concurrent droughts and heatwaves in the United States. *Proc. Natl. Acad. Sci. U.S.A.* **112**, 11484–11489 (2015).
16. J. L. Geirinhas *et al.*, Recent increasing frequency of compound summer drought and heatwaves in Southeast Brazil. *Environ. Res. Lett.* **16**, 034036 (2021).
17. T. Cowan *et al.*, More frequent, longer, and hotter heat waves for Australia in the Twenty-First century. *J. Clim.* **27**, 5851–5871 (2014).
18. S. C. Lewis, D. J. Karoly, Anthropogenic contributions to Australia's record summer temperatures of 2013. *Geophys. Res. Lett.* **40**, 3705–3709 (2013).
19. K.-J. Ha *et al.*, Dynamics and characteristics of dry and moist heatwaves over East Asia. *Npj Clim. Atmos. Sci.* **5**, 1–11 (2022).
20. S. Sharma, P. Mujumdar, Increasing frequency and spatial extent of concurrent meteorological droughts and heatwaves in India. *Sci. Rep.* **7**, 15582 (2017).
21. X. Wu, Z. Hao, Y. Zhang, X. Zhang, F. Hao, Anthropogenic influence on compound dry and hot events in China based on Coupled Model Intercomparison Project Phase 6 models. *Int. J. Climatol.* **42**, 4379–4390 (2022).
22. R. Yu, P. Zhai, More frequent and widespread persistent compound drought and heat event observed in China. *Sci. Rep.* **10**, 14576 (2020).
23. Z. Hao, A. AghaKouchak, T. J. Phillips, Changes in concurrent monthly precipitation and temperature extremes. *Environ. Res. Lett.* **8**, 034014 (2013).
24. E. Bevacqua, G. Zappa, F. Lehner, J. Zscheischler, Precipitation trends determine future occurrences of compound hot–dry events. *Nat. Clim. Change* **12**, 350–355 (2022).
25. G. Konapala, A. K. Mishra, Y. Wada, M. E. Mann, Climate change will affect global water availability through compounding changes in seasonal precipitation and evaporation. *Nat. Commun.* **11**, 3044 (2020).
26. S. Mukherjee, M. Ashfaq, A. K. Mishra, Compound drought and heatwaves at a global scale: The role of natural climate variability-associated synoptic patterns and land-surface energy budget anomalies. *J. Geophys. Res. Atmos.* **125**, e2019JD031943 (2020).
27. D. G. Miralles, P. Gentine, S. I. Seneviratne, A. J. Teuling, Land–atmospheric feedbacks during droughts and heatwaves: State of the science and current challenges. *Ann. N. Y. Acad. Sci.* **1436**, 19–35 (2019).
28. A. Sarhadi, M. C. Ausín, M. P. Wiper, D. Touma, N. S. Diffenbaugh, Multidimensional risk in a nonstationary climate: Joint probability of increasingly severe warm and dry conditions. *Sci. Adv.* **4**, eaau3487 (2018).
29. E. M. Fischer, S. Sippel, R. Knutti, Increasing probability of record-shattering climate extremes. *Nat. Clim. Change* **11**, 689–695 (2021).
30. Q. Zhang *et al.*, High sensitivity of compound drought and heatwave events to global warming in the future. *Earths Future* **10**, e2022EF002833 (2022).
31. B. I. Cook *et al.*, Uncertainties, limits, and benefits of climate change mitigation for soil moisture drought in Southwestern North America. *Earths Future* **9**, e2021EF002014 (2021).
32. R. Seager *et al.*, Model projections of an imminent transition to a more arid climate in Southwestern North America. *Science* **316**, 1181–1184 (2007).
33. J. E. Herrera-Estrada *et al.*, Reduced moisture transport linked to drought propagation across North America. *Geophys. Res. Lett.* **46**, 5243–5253 (2019).
34. J. Singh *et al.*, Enhanced risk of concurrent regional droughts with increased ENSO variability and warming. *Nat. Clim. Change* **12**, 163–170 (2022).
35. Y. Kosaka, S.-P. Xie, Recent global-warming hiatus tied to equatorial Pacific surface cooling. *Nature* **501**, 403–407 (2013).
36. M. A. Balmaseda, K. E. Trenberth, E. Källén, Distinctive climate signals in reanalysis of global ocean heat content. *Geophys. Res. Lett.* **40**, 1754–1759 (2013).
37. F. Estrada, P. Perron, B. Martínez-López, Statistically derived contributions of diverse human influences to twentieth-century temperature changes. *Nat. Geosci.* **6**, 1050–1055 (2013).
38. I. P. Change, on C., "Climate change 2013: The physical science basis: Working group I contribution to the fifth assessment report of the intergovernmental panel on climate change" (Cambridge University Press, Cambridge, United Kingdom and New York, USA, 2014), pp. 1535.
39. M. M. Vogel *et al.*, Regional amplification of projected changes in extreme temperatures strongly controlled by soil moisture-temperature feedbacks. *Geophys. Res. Lett.* **44**, 1511–1519 (2017).
40. W. Cai *et al.*, Increasing frequency of extreme El Niño events due to greenhouse warming. *Nat. Clim. Change* **4**, 111–116 (2014).
41. D. G. Miralles, A. J. Teuling, C. C. van Heerwaarden, J. Vilà-Guerau de Arellano, Mega-heatwave temperatures due to combined soil desiccation and atmospheric heat accumulation. *Nat. Geosci.* **7**, 345–349 (2014).
42. R. Lorenz, E. B. Jaeger, S. I. Seneviratne, Persistence of heat waves and its link to soil moisture memory. *Geophys. Res. Lett.* **37**, L09703 (2010).
43. V. Petoukhov *et al.*, Role of quasiresonant planetary wave dynamics in recent boreal spring-to-autumn extreme events. *Proc. Natl. Acad. Sci. U.S.A.* **113**, 6862–6867 (2016).
44. M. E. Mann *et al.*, Influence of anthropogenic climate change on planetary wave resonance and extreme weather events. *Sci. Rep.* **7**, 45242 (2017).
45. M. E. Mann *et al.*, Projected changes in persistent extreme summer weather events: The role of quasi-resonant amplification. *Sci. Adv.* **4**, eaat3272 (2018).
46. A. P. Williams, C. Funk, A westward extension of the warm pool leads to a westward extension of the Walker circulation, drying eastern Africa. *Clim. Dyn.* **37**, 2417–2435 (2011).
47. F. Giorgi *et al.*, Changes in extremes and hydroclimatic regimes in the CREMA ensemble projections. *Clim. Change* **125**, 39–51 (2014).
48. C. Funk *et al.*, Recent drought tendencies in ethiopia and equatorial subtropical Eastern Africa: Famine Early Warning System Network Special Report. (US Agency for International Development, 2005), pp. 12.
49. P. J. Reddy, S. E. Perkins-Kirkpatrick, N. N. Ridder, J. J. Sharples, Combined role of ENSO and IOD on compound drought and heatwaves in Australia using two CMIP6 large ensembles. *Weather Clim. Extrem.* **37**, 100469 (2022).
50. T. Ambrizzi, M. S. Reboita, R. P. da Rocha, M. Llopart, The state of the art and fundamental aspects of regional climate modeling in South America. *Ann. N. Y. Acad. Sci.* **1436**, 98–120 (2019).
51. M. E. Mann, Beyond the hockey stick: Climate lessons from the Common Era. *Proc. Natl. Acad. Sci. U.S.A.* **118**, e2112797118 (2021).
52. X. He, M. Pan, Z. Wei, E. F. Wood, J. Sheffield, A global drought and flood catalogue from 1950 to 2016. *Bull. Am. Meteorol. Soc.* **101**, E508–E535 (2020).
53. G. Konapala, A. Mishra, Quantifying climate and catchment control on hydrological drought in the continental United States. *Water Resour. Res.* **56**, e2018WR024620 (2020).
54. M. R. Alizadeh *et al.*, A century of observations reveals increasing likelihood of continental-scale compound dry-hot extremes. *Sci. Adv.* **6**, eaaz4571 (2020).
55. F. Shadman, S. Sadeghipour, M. Moghavvemi, R. Saidur, Drought and energy security in key ASEAN countries. *Renew. Sustain. Energy Rev.* **53**, 50–58 (2016).
56. B. Su *et al.*, Drought losses in China might double between the 1.5 °C and 2.0 °C warming. *Proc. Natl. Acad. Sci. U.S.A.* **115**, 10600–10605 (2018).
57. G. Naumann, C. Cammalleri, L. Mentaschi, L. Feyen, Increased economic drought impacts in Europe with anthropogenic warming. *Nat. Clim. Change* **11**, 485–491 (2021).
58. Y. Zhang, P. Yang, Y. Gao, R. L. Leung, M. L. Bell, Health and economic impacts of air pollution induced by weather extremes over the continental U.S. *Environ. Int.* **143**, 105921 (2020).
59. L. R. Prugh *et al.*, Ecological winners and losers of extreme drought in California. *Nat. Clim. Change* **8**, 819–824 (2018).
60. C. Miao, L. Su, Q. Sun, Q. Duan, A nonstationary bias-correction technique to remove bias in GCM simulations. *J. Geophys. Res. Atmos.* **121**, 5718–5735 (2016).
61. R. Webb, C. E. Rosenzweig, E. R. Levine, Global soil texture and derived water-holding capacities (Webb et al.). ORNL DAAC (2000), 10.3334/ORNLDAAC/548.
62. N. Wells, S. Goddard, M. J. Hayes, A self-calibrating palmer drought severity index. *J. Clim.* **17**, 2335–2351 (2004).
63. N. Devineni, A. Sankarasubramanian, Improved categorical winter precipitation forecasts through multimodel combinations of coupled GCMs. *Geophys. Res. Lett.* **37**, L24704 (2010).
64. N. N. Ridder *et al.*, Global hotspots for the occurrence of compound events. *Nat. Commun.* **11**, 5956 (2020).
65. C.-F. Schleussner *et al.*, Science and policy characteristics of the Paris Agreement temperature goal. *Nat. Clim. Change* **6**, 827–835 (2016).
66. C.-E. Park, S. Jeong, Population exposure projections to intensified summer heat. *Earths Future* **10**, e2021EF002602 (2022).
67. S. I. Seneviratne, M. Hauser, Regional climate sensitivity of climate extremes in CMIP6 versus CMIP5 multimodel ensembles. *Earths Future* **8**, e2019EF001474 (2020).